Title

Restriction spectrum imaging: An evolving imaging biomarker in prostate MRI.

Journal

Journal of magnetic resonance imaging : JMRI, 45(2)

ISSN

1053-1807

Authors

Brunsing, Ryan L
Schenker-Ahmed, Natalie M
White, Nathan S
et al.

Publication Date

2017-02-01

DOI

10.1002/jmri.25419

Peer reviewed

Restriction Spectrum Imaging: An Evolving Imaging Biomarker in Prostate MRI

Ryan L. Brunsing, MD, PhD,[1] Natalie M. Schenker-Ahmed, PhD,[1] Nathan S. White, PhD,[1] J. Kellogg Parsons, MD, MHS,[2] Christopher Kane, MD,[2] Joshua Kuperman, PhD,[1] Hauke Bartsch, PhD,[1] Andrew Karim Kader, MD, PhD,[2] Rebecca Rakow-Penner, MD, PhD,[1] Tyler M. Seibert, MD, PhD,[3] Daniel Margolis, MD,[4] Steven S. Raman, MD,[4] Carrie R. McDonald, PhD,[5] Nikdokht Farid, MD,[1] Santosh Kesari, MD, PhD,[6] Donna Hansel, MD, PhD,[7] Ahmed Shabaik, MD,[7] Anders M. Dale, PhD,[1,8] and David S. Karow, MD, PhD[1]*

Restriction spectrum imaging (RSI) is a novel diffusion-weighted MRI technique that uses the mathematically distinct behavior of water diffusion in separable microscopic tissue compartments to highlight key aspects of the tissue microarchitecture with high conspicuity. RSI can be acquired in less than 5 min on modern scanners using a surface coil. Multiple field gradients and high b-values in combination with postprocessing techniques allow the simultaneous resolution of length-scale and geometric information, as well as compartmental and nuclear volume fraction filtering. RSI also uses a distortion correction technique and can thus be fused to high resolution T2-weighted images for detailed localization, which improves delineation of disease extension into critical anatomic structures. In this review, we discuss the acquisition, postprocessing, and interpretation of RSI for prostate MRI. We also summarize existing data demonstrating the applicability of RSI for prostate cancer detection, in vivo characterization, localization, and targeting.
Level of Evidence: 5

J. MAGN. RESON. IMAGING 2017;45:323–336

Prostate cancer (PCa) is the most common noncutaneous malignancy in males and the second leading cause of cancer-related death among men in the United States,[1] with an estimated one in six American men diagnosed with PCa in their lifetime.[2] MRI has demonstrated potential value for PCa staging, treatment planning, and follow-up.[3–8] However, suboptimal sensitivity and specificity and inconsistency in identifying foci of high-grade disease highlight that current MRI protocols remain suboptimal for cancer detection, staging, and in vivo characterization.[9–12] Thus, more robust diagnostic tools are needed to maximize the potential of this promising imaging modality.

Advances in MR scanner technology have allowed the development of powerful MRI sequence protocols that highlight specific biophysical properties of tissue. One such technique is diffusion-weighted MRI (DWI), which detects limitations in the microscopic movement of water molecules due to tissue architecture. DWI has a high conspicuity for PCa relative to normal tissue,[8–21] and when combined with T2-weighted imaging offers higher sensitivity and specificity in cancer detection (0.76 and 0.94, respectively) as compared to T2-weighted images alone (0.61 and 0.91, respectively).[10] Based on an abundance of supporting data, the

View this article online at wileyonlinelibrary.com. DOI: 10.1002/jmri.25419

Received May 24, 2016, Accepted for publication Jul 25, 2016.

*Address reprint requests to: D.S.K., Multimodal Imaging Laboratory (MMIL), 8950 Villa La Jolla Dr., Suite C101, La Jolla, CA 92037. E-mail: dkarow@ucsd.edu

From the [1]Department of Radiology, University of California San Diego, San Diego, California, USA; [2]Department of Surgery, University of California San Diego, San Diego, California, USA; [3]Department of Radiation Medicine, University of California San Diego, San Diego, California, USA; [4]Department of Radiology, University of California Los Angeles, Los Angeles, California, USA; [5]Department of Psychiatry, University of California San Diego, La Jolla, California, USA; [6]Department of Translational Neuro-Oncology and Neurotherapeutics, Pacific Neuroscience Institute and John Wayne Cancer Institute at Providence Saint John's Health Center, Los Angeles, California, USA; [7]Department of Pathology, University of California San Diego, San Diego, California, USA; and [8]Department of Neurosciences, University of California San Diego, La Jolla, California, USA

Drs. Brunsing and Schenker-Ahmed contributed equally to this work.

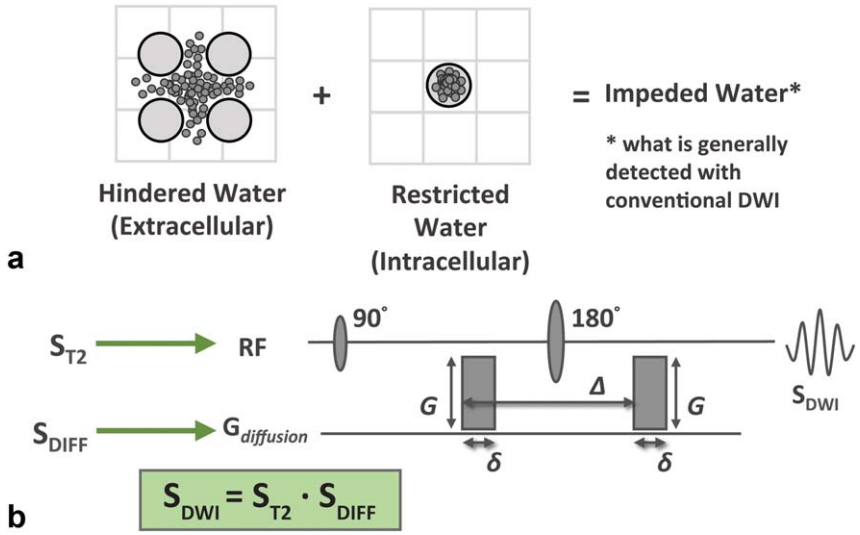

FIGURE 1: Foundations of DWI. A: Water within tissue can be confined to the intracellular or extracellular compartment, the intracellular water having a limited range determined by the configuration of the plasma membrane. The combined signal from both is measured in conventional DWI and referred to as impeded water. B: Standard spin-echo echo-planar pulse sequence used in conventional diffusion weighted imaging. It is important to note that signal from diffusion imaging represents the sum effect of both the diffusion and T2 properties of the tissue being probed.

recently released American College of Radiology guidelines for PCa MRI interpretation, PI-RADS version 2 (PIRADSv2), uses DWI as the core sequence for assessing peripheral zone lesions.[22,23] Current standard-of-care PCa MRI also includes a dynamic contrast enhanced imaging (DCE) and anatomic T1 and T2-weighted (T1w and T2w) sequences in addition to DWI. Despite its clinical utility, there are some notable limitations of conventional DWI. Information from the T2 component of the signal is not used; information about the underlying geometry is not obtained; signal from intracellular and extracellular water is mixed; and inherent spatial distortion issues caused by field inhomogeneities are not addressed.

A recently developed advanced diffusion-based technique termed restriction spectrum imaging (RSI) attempts to address many of these limitations.[24] In this review, we discuss the acquisition, postprocessing, and interpretation of RSI in the setting of prostate cancer. We also summarize existing data demonstrating the applicability of RSI for prostate cancer detection, in vivo characterization, localization, and targeting

Principles of Diffusion Weighted Imaging

Signal in DWI is inversely related to the net movement of water within the tissue being probed. Water molecules spread apart due to random motion driven by thermal energy. In pure solution they will disperse in a predictable way following a Gaussian distribution in a process called "free diffusion." However, in biological tissues the process is more complex. Water diffusion can be impeded by one of two general mechanisms: hindrance by the physical boundaries of the extracellular space (predominantly determined by the geometric tortuosity associated with the cell packing density – see Fig. 1A) or restriction of water within the intracellular compartment (Fig. 1A). *For discussion purposes in this paper, restricted diffusion refers specifically to water trapped within the intracellular space*, as defined classically,[25,26] and "impeded diffusion" refers to the collective signal from restricted and hindered compartments. By this definition, conventional DWI generally reflects signal attenuation due to impeded diffusion, noting that increased sensitivity to restricted diffusion can be achieved with increasing diffusion-weighting (b-value, see below).

There are two discrete properties of diffusion that can be measured using diffusion-based techniques. The first is the length-scale distribution, reflecting the scalar distance that water is able to travel over a given time (e.g., the diffusion time). The second is orientation or geometric information, reflecting preferential diffusion vectors in three-dimensional (3D) space resulting from regional tissue architecture (for example water will tend to travel along an axon rather than through its membrane). In general, the mathematical frameworks used for current clinical diffusion-based MRI protocols calculate one of these two diffusion properties at the expense of the other. MR tractography, such as diffusion tensor imaging (DTI), is an example of a clinical diffusion-based technique that collects geometric information.[27]

Most conventional DWI protocols are based on the classic Stejskal-Tanner single-shot pulsed-gradient spin-echo (PGSE) technique[28] which measures length-scale distribution properties. In this sequence, signal is generated from a "root" spin-echo sequence where the inversion pulse is flanked by diffusion gradients of strength G for a duration δ separated by a time Δ (Fig. 1B). The first gradient serves to encode the initial physical position of the water molecule relative to the gradient field and the second gradient serves as a refocusing pulse. Increased movement of water (by

means of diffusion) along the diffusion gradient axis in the time Δ results in decreased signal due to increasingly ineffective refocusing. Thus impeded water movement results in a less attenuated (or relatively increased) diffusion signal compared with free water.

An important aspect of the PGSE sequence, which is often overlooked, is that it is a T2-weighted sequence. This means that the strength of the DWI signal within a given voxel is determined by both the degree of diffusion and the inherent T2 of the tissues therein. Mathematically, the signal from DWI (S_{DWI}) is equal to the intrinsic T2-weighted signal of the tissue (S_{T2}) multiplied by the diffusion gradient effects (S_{DIFF}) described in the preceding paragraph.

$$\mathbf{S_{DWI} = S_{T2} \cdot S_{DIFF}}$$

(see Fig. 1B)

To distinguish between the two sources of DWI signal, images are compared with apparent diffusion coefficient (ADC) maps, calculated from a mathematical framework proposed by Stejskal and Tanner in 1965.[28] Lower ADC values represent true impeded diffusion, while high signal on both DWI and ADC represent T2 shine-through. In the Stejskal and Tanner model, signal from the diffusion component (S_{DIFF}) decays exponentially according to the ADC value, encompassing the length-based diffusion properties of the system, and the b-value, encompassing effects of the machine-controlled parameters:

$$\mathbf{S_{DIFF} = S_0 \cdot e^{-(b \cdot ADC)}}$$

$$\mathbf{b = (G^2 \cdot \gamma^2 \cdot \delta^2) \cdot (\Delta - \delta/3)}$$

where S_0 is the signal at b = 0 and γ = the Lamor frequency of protons remaining parameters defined in Figure 1B.

Decay of the diffusion component of the signal (S_{DIFF}) can be enhanced by increasing the b value, which may be achieved by increasing the diffusion time Δ, gradient strength G, or both. In this setting, only tissues that have high levels of impeded water will retain signal. These properties explain why DWI has been so widely investigated as a tool for oncologic imaging: highly cellular tumors have increased volumes of restricted intracellular water and should theoretically exhibit high signal on conventional DWI and low values on the quantifiable ADC maps.

While powerful, this framework has several limitations: As a composite measure, the standard DWI measurement of the apparent diffusion coefficient (ADC) reflects the average molecule displacements of water molecules within the imaging voxel and does not differentiate diffusion signals stemming from separable tissue sub-compartments (e.g. intracellular and extracellular spaces). This limitation in the ability to distinguish signals from different sub-compartments likely contributes to the suboptimal sensitivity and specificity of ADC in discriminating cancer from healthy tissue.[9–12] This issue is further compounded in the setting of iatrogenic changes to the tumor microenvironment such as postbiopsy hemorrhage.[29] Additionally, DWI does not take advantage of information from the T2 component of the signal nor the geometric information embedded in the mechanism of signal acquisition. Finally, conventional DWI images are subject to significant distortion from B_0 magnetic field inhomogeneities created by material interfaces, patient geometry, and eddy currents,[30] limiting DWI's role in discerning anatomic localization for biopsy, cancer staging, and treatment planning.

Restriction Spectrum Imaging Theory and Acquisition

The major advantage of RSI over most other diffusion techniques is that it uses diffusion data collected with multiple gradient directions and b-values (termed a "multi-shell" acquisition), together with an advanced linear mixture model to resolve a spectrum of length scales (hence, "restriction spectrum imaging")[25] while simultaneously acquiring geometric information.[24] This is accomplished using a linear mathematical framework allowing reasonable computation times. In addition, because the multi-shell sequence acquisition used for RSI captures information across a broader set of variables than conventional DWI, RSI has the potential to be normalized across institutions, unlike ADC, which remains machine and technique dependent. In the future, this may eliminate one of the major roadblocks that have undermined clinical application of ADC maps.

For prostate MRI, RSI is used to separate restricted diffusion within small spherical cells from extra-cellular hindered and free water compartments. RSI cellularity index (RSI CI), derived from the spherically restricted diffusion signal, has demonstrated correlation to the nuclear-cytoplasmic ratio in a simulated cancer cell model[28] and shows great promise as a quantitative imaging biomarker. Finally, RSI incorporates an advanced postprocessing technique for distortion correction based on the reverse phase encode method[29] that allows for accurate colocalization with fast spin-echo T2-weighted sequences for discrete anatomic precision.[30–32] Importantly, RSI maintains the many strengths of conventional DWI, including high signal-to-noise ratio (SNR) and does not require a separate pulse-sequence or additional scan time. The mathematical foundations of RSI have previously been described in detail by White et al.[24] That manuscript also includes a discussion of other advanced diffusion-based techniques.

Protocol

The current institutional prostate RSI protocol uses non-zero b-values of 125, 375, and 1000 s/mm^2 with 6, 6, and 15 diffusion gradients, respectively (Table 1 and Fig. 2A) using a cardiac coil on a 3.0 Tesla (T) GE (Milwaukee, WI) platform. Following postprocessing (described below), RSI Cellularity Maps, acquired using the parameters outlined in Table 1, are

TABLE 1. Prostate RSI Protocol

Coil: cardiac, no endorectal coil is required
Repetition time: 9900 ms
Echo time: 69-72 ms
Field of View: 200-260 mm
Matrix: 96×96
Slice thickness: 3.0 mm
b values (s/mm^2):
0: alternate phase encoding direction for distortion correction
125: 6 diffusion gradient directions
375: 6 diffusion gradient directions
1000: 15 diffusion gradient directions

fused to axial T2w images. Currently, all patients who undergo prostate MRI at our institution receive RSI as part of their exam in addition to current standard-of-care sequences; axial T2w images, axial dynamic contrast enhanced images (DCE), and axial DWI images (b = 0 and 1000) with ADC map reconstruction. For purposes of discussion, this collective protocol will be referred to as mpMRI+RSI. Furthermore, any patients referred to our institution for prostate MRI receive RSI as part of their exam. To date, RSI has been acquired on both GE and Siemens (Erlangen, Germany) 3T scanners.

RSI Postprocessing in PCA

Compartmental Filtering

As discussed above conventional DWI does not reliably and predictably differentiate between the intracellular and extracellular water compartments, which demonstrate distinct diffusion properties (S_{DIFF}) and T2 signal characteristics (S_{T2}), and likely have distinct implications in tumor detection, characterization, localization, and treatment. Signal diffusion-based techniques, including RSI (S_{RSI}), is the sum of unique signals from the hindered (S_H) and restricted compartments (S_R) as well as signal from free water (S_F):

$$\mathbf{S_{DWI/RSI}} = \mathbf{S_H}(\text{Hindered}) + \mathbf{S_R}(\text{Restricted}) + \mathbf{S_F}(\mathbf{Free}).$$

Upon closer investigation into the diffusion characteristics of the two compartments (Fig. 2A), it is clear that water in the extracellular compartment has essentially unlimited range to travel, while intracellular water is confined by the walls of the cell. (Note: in reality there is exchange of water between the intra- and extracellular compartments, however, on the time scales used in RSI exchange effects are small.[31]) Therefore, as one increases the diffusion weighting, e.g., by increasing the diffusion time Δ, signal drops out more quickly in the extracellular compartment. At high b values, signal from intracellular water can be isolated (Fig. 2A). In this setting, increasing signal correlates with increasing intracellular water and thus tissue cellularity (Fig. 2B). RSI uses multiple b-values to separate a spectrum of length-scales, which correlate with distinct compartments within a tissue. In the setting of PCa, signal from this highly restricted intracellular compartment is highlighted. This concept forms one of the two foundations of PCa RSI cellularity maps.

Geometric Filtering

The second foundation for RSI cellularity maps comes from the ability to simultaneously separate water fractions based on geometric information. Using advanced postprocessing

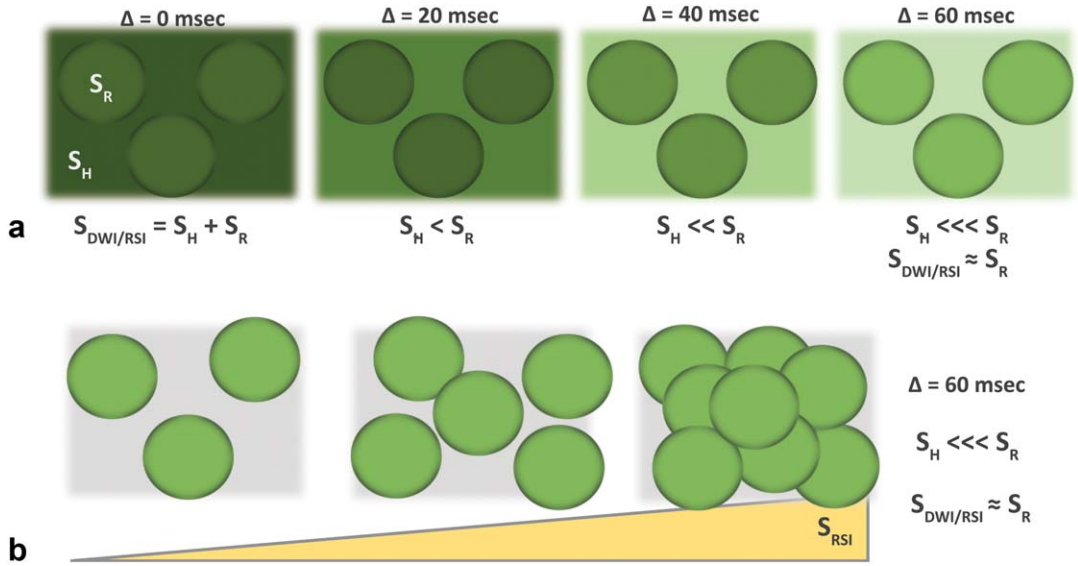

FIGURE 2: Foundations of RSI, compartmental filtering. A: With time, the signal from hindered water dissipates more quickly than that from restricted water (darker green indicates greater signal). B: Signal from RSI increases with greater cell density.

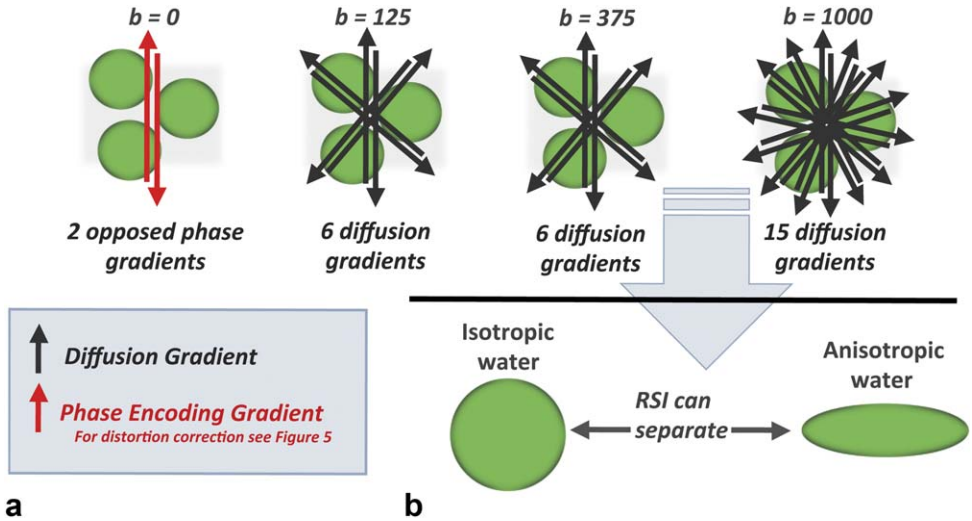

FIGURE 3: Foundations of RSI, geometric filtering. A: Schematic outlining the basic parameters of the RSI multishell acquisition, with opposed phase encoding gradients in the b = 0 acquisition used for distortion correction and 6, 6, and 15 nonparallel gradients for the non-zero b values. B: Using this data, RSI can simultaneously acquire length-scale distribution data and geometric information, allowing isolation of isotropic and anisotropic orientation data. In prostate cancer, RSI is used to isolate signal from highly restricted and isotropic water.

techniques discussed,[24,32,33] the high number of distinct gradient directions (Fig. 3A) allows for water exhibiting isotropic (spherical) diffusion (as would be seen within tumor cell that is small and round, for example) to be distinguished from water exhibiting anisotropic (cylindrical) diffusion (as would be seen in axons, for example), similar to the diffusion tensor based techniques used in tractography[27] (Fig. 3B). For PCa, RSI cellularity maps represent isotropic diffusion signal.

In summary, RSI uses a range of high b-values and multiple diffusion gradients to simultaneously separate multiple length-scales / compartments and geometric information, respectively. In the setting of PCa, RSI cellularity maps are tuned to highlight signal from highly restricted spherical compartments of water, such as those expected in small round tumor cells.

Nuclear Volume Fraction filtering

The concept of an imaging biomarker centers on the usage of quantitative information derived from medical imaging to guide preclinical development and clinical decision making.[34] Imaging biomarkers hold great promise in personalized cancer care,[35] where matching the patient to the appropriate therapeutic regimen will become increasingly complex and important. Despite a great deal of focus on the use of ADC as an imaging biomarker in oncology,[36] overlap between theoretical reference ranges[37] and confounding results[38] continue to make clinical guidance using ADC values untenable. New techniques are needed to build upon the promising, but thus far unrealized, quantitative potential of diffusion-based imaging.

In PCa, one area where imaging biomarkers could provide valuable clinical guidance would be in predicting Gleason grade. RSI approaches this by using the T2 properties of the intracellular space. The inherent T2 values of the nucleus and cytoplasm differ substantially measuring approximately 65 ms and 25 ms, respectively[31] (Fig. 4A). As the ratio of nuclear to cytoplasmic space increases, the percentage of intracellular water contained within the nucleus correspondingly increases. This percentage has previously been termed the nuclear volume fraction (NVF),[33] and correlates with the histopathologic concept nuclear-to-cytoplasmic ratio.

As NVF increases, the effective T2 of the intracellular space and thus the signal S_{T2} also increase (Fig. 4B). Note that the diffusion characteristics (S_{DIFF}) of the nucleus and cytoplasm are the same. Therefore, when the underlying cellularity remains unchanged, increased signal within a voxel on the RSI cellularity map represents a proportional increase in NVF within that voxel (Fig. 4B) due to increasing S_{T2}. An example is provided in Figure 4c. The glioblastoma in the left panel (WHO grade 4) demonstrates high signal on the RSI Cellularity map, correlating with the small isotropic cells seen on the histopathological section and with a high NVF.

Conversely, there is minimal RSI signal on the WHO grade 2 glioma in the right panel, correlating with the lower NVF seen on the histopathological section. By normalizing to remove effects from the diffusion component, NVF can be mathematically estimated from RSI cellularity map (RSI-CM) data acquired at multiple echo times. Within this framework, one would theoretically expect the RSI Z-scores (referred to as "cellularity index,"[39] calculated below) to correlate with NVF. Preliminary data obtained from the application of prostate MRI suggests that this is true[40,41] as discussed below. This represents a major advancement beyond current DWI, which is indifferent to intracellular changes in histopathologic architecture.

In practice, the approach has been to calculate the mean value (MV_N) and standard deviation (SD_N) of RSI

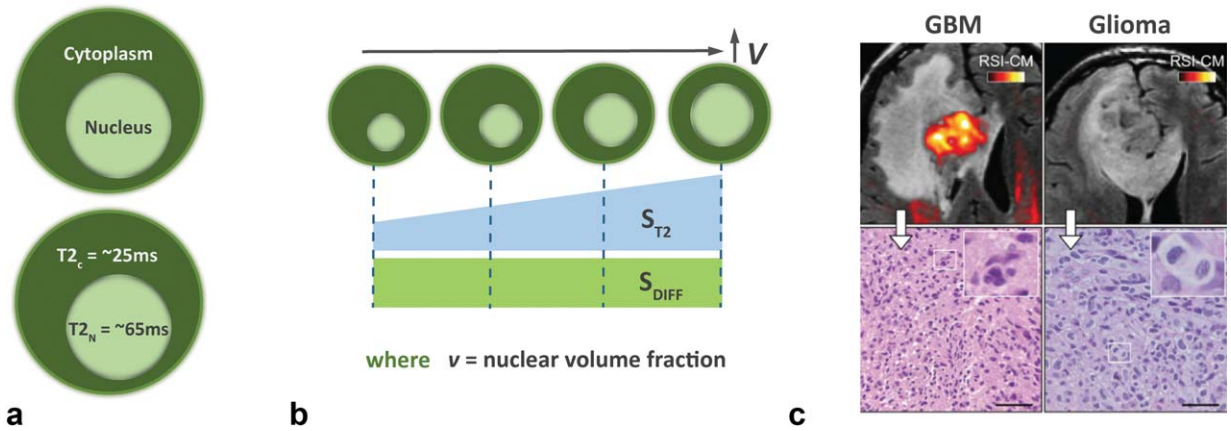

FIGURE 4: Foundations of RSI, nuclear volume fraction. A: The inherent T2 signal of the cytoplasm and nucleus differ substantially. B: Increasing nuclear volume fraction (NVF) results in a corresponding increase in effective T2. As the nucleus and cytoplasm exhibit similar diffusion properties, this change in effective T2 can be measured and used to calculate NVF.

signal per voxel from a normal region of the tissue in question. This can be done from individual or pooled patient data. The RSI cellularity index (CI) (representing the Z-score) can then be calculated as:

$$\text{RSI CI} = (\text{RSI-CM VOXEL SIGNAL} - \text{MV}_N)/\text{SD}_N$$

Distortion Correction

DWI is prone to image distortion due to B_0 magnetic field inhomogeneities.[30,33] Distortion can lead to misregistration of signal by up to 13 mm[32] and is of particular importance in the phase-encoding direction because of the time between sample points. This carries large implications for cancer staging.[42] Dilemmas at critical treatment decision points can arise when tumor margins approach important anatomic landmarks or when suspicious lesions detected outside the primary mass do not declare themselves as benign or malignant. To address this, RSI uses a distortion correction technique based on the acquisition of $b = 0$ images with opposite phase encoding polarizations[43] (Fig. 5A). This technique has been applied to the PCa RSI protocol[32] and

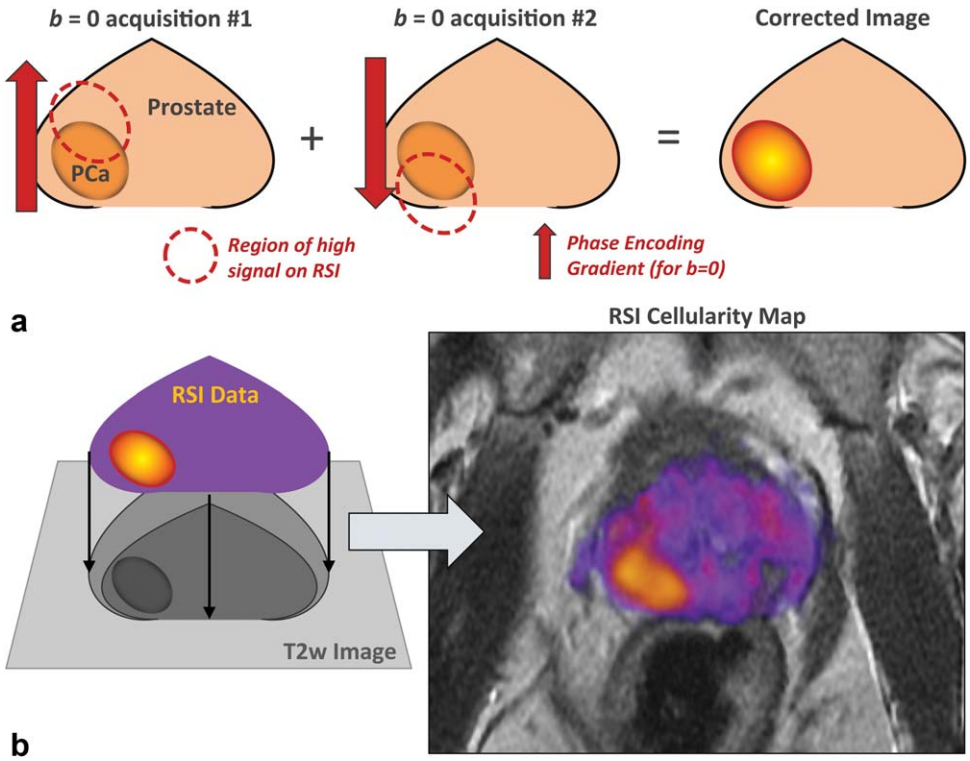

FIGURE 5: Foundations of RSI, distortion correction. Opposed phase encode gradients are used to cancel out distortion caused by magnetic field inhomogeneities (A), allowing for the fusion of RSI cellularity maps with high resolution anatomic images (B). These fused images are the foundation of clinical RSI interpretation.

TABLE 2. Advantages of RSI

	Compartmental filtering	Geometric filtering	Nuclear fraction	Distortion correction
DWI/ADC	Possible	No	No	Possible
RSI	Yes	Yes	Yes	Yes

DWI = diffusion-weighted imaging; ADC = apparent diffusion coefficient; RSI = restriction spectrum imaging.

others, allowing RSI cellularity maps to be fused to high resolution T2-weighted sequences for detailed anatomic localization (Fig. 5B) on a voxel-by-voxel level.

In PCa, distortion correction is particularly valuable for identifying extra-prostatic extension (EPE) beyond the capsule, which has important staging and surgical implications.[5,42] In a proof of concept study by Rakow-Penner et al, fused T2-RSI images with distortion correction demonstrated improved sensitivity for EPE in prostate cancer patients (8/9, 89%) versus standard of care mpMRI alone (2/9, 22%).[44] Notably, this was a nonblinded pilot study with small patient numbers. While theoretically possible to apply to conventional DWI, most current clinical protocols do not use distortion correction.

Summary of Filtering Techniques

For prostate MRI, RSI provides a direct estimate of tissue cellularity by isolating signal from isotropic intracellular water, uses T2 signal characteristics to provide quantitative information about nuclear volume fraction, and incorporates distortion correction techniques allowing fusion of RSI cellularity maps with high spatial resolution imaging. While the first and last of these are theoretically possible with conventional DWI, they are not widely used. The other two, which represent advancements for quantitative imaging, are unique to RSI. A comparison of the two approaches can be found in Table 2.

Interpretation of Prostate MRI with RSI: Existing Data

Next follows a summary of publications to date demonstrating the utility of RSI as an imaging biomarker for prostate cancer detection, in vivo characterization, and localization/targeting.

Cancer Detection

Cancer treatment begins with cancer detection. Diffusion-based techniques are attractive as a tool in cancer detection given their high conspicuity and fast acquisition and have already proven clinical utility in prostate cancer.[3–6,8–16] However, as noted earlier, these techniques remain marred by several limitations including suboptimal sensitivity and specificity.[9–12]

The power of RSI as a tool for cancer detection was initially demonstrated by work with intracranial neoplasms. In a study evaluating 10 patients with CNS malignancy, RSI demonstrated (i) increased tumor conspicuity and (ii) greater sensitivity/specificity (based on receiver-operating characteristic curve data) in delineating malignant tissue from normal white matter tracts (which can also exhibit some degree of impeded diffusion) as compared to DWI images and ADC maps derived from b-values of 500, 1500, and 4000.[49] Additionally, bevacizumab treatment of intracranial neoplasms can be associated with regions of persistent DWI signal despite elimination of the underlying tumor, so called bevacizumab-related imaging abnormalities (BRIA).[50] In fact, the presence of impeded diffusion following bevacizumab treatment of malignant gliomas correlated with improved overall survival,[51] suggesting prognostic value. RSI demonstrated increased sensitivity in detecting areas of persistent restricted diffusion relative to conventional DWI, and when combined with relative cerebral blood volume measurements may be able to differentiate BRIA from residual tumor.[45,46] Prior manuscripts have presented and discussed the promising results using RSI in intracranial neoplasms.[33,45–48]

In PCa, McCammack et al directly compared the detection capacity of RSI cellularity maps to that of quantitative maps from current mpMRI sequences,[40] namely DWI (ADC) and DCE (K^{trans}, K_{ep}, and V_e). Tumors were defined and graded by an experienced uropathologist using thin whole-mount sections from 33 patients who underwent preoperative mpMRI+RSI before radical prostatectomy. Corresponding regions of interest (ROIs) were drawn on T2w images by an experienced radiologist, and subsequently cross referenced to the above quantitative maps for direct comparison of histopathological results and imaging data. RSI CI significantly outperformed ADC values in differentiating tumor from normal tissue. Both RSI and ADC significantly outperformed DCE-based measures[40] (Fig. 6). The MRIs in this study were acquired using a current clinical-grade protocol with a cardiac surface coil on a GE platform. No bowel prep or endorectal coil was required. These results demonstrate that RSI can outperform current mpMRI tools in detecting PCa as assessed by direct comparison to histopathological data.

To evaluate the clinical performance of RSI in PCa detection, McCammack et al conducted a retrospective

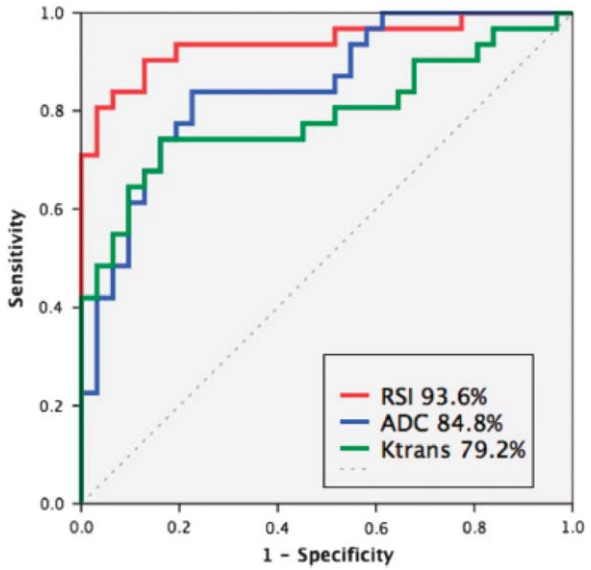

FIGURE 6: Receiver-operating characteristic curves for the quantitative discrimination of prostate cancer from normal peripheral zone. Areas under the curve are listed in the legend. Used with permission from McCammack et al. *PCAN*, 2016.[40]

study of 100 patients (67 with pathologically proven prostate cancer, 30 of which were high-grade) who underwent mpMRI+RSI within 6 months of systematic biopsy or prostatectomy.[41] Studies were reviewed by three independent radiologists.[41] Analysis at both the sextant and hemigland level demonstrated that mpMRI with RSI (area under the receiver operating characteristics curve [AUC] 0.69 and 0.71, respectively) outperformed mpMRI alone (AUC 0.63 and 0.68). At the sextant level, the independent performance of all three readers was significantly improved with the incorporation of RSI. Moreover, inter-reader agreement was higher when RSI was added to mpMRI. These results demonstrate that RSI-MRI can outperform current standard of care mpMRI in the clinical setting as well.

Additional data from this same study may have implications for PCa screening programs. Population screening with serum prostate specific antigen (PSA) testing reduces prostate cancer mortality, but is limited by PSA's relatively low specificity, which can lead to PCa over-detection and over-treatment.[52] In an abbreviated MR protocol using RSI and T2 (RSI+T2) in the same cohort of 100 patients, RSI+T2 was found to be at least as effective as conventional mpMRI in detecting high-grade PCa (primary Gleason grade ≥ 4). Moreover, variability in reader interpretations was the lowest when RSI was evaluated in isolation, possibly due to the increased conspicuity that makes RSI images easier to read. Notably, this RSI+T2 protocol does not require administration of contrast and can be acquired in less than 10 min on a GE Signa HDxt 3.0T machine using a cardiac surface coil. Use of a more modern scanner would reduce the time required even further. The combination of robust delineation of disease, reproducibility of interpretation, and ease of acquisition make this limited protocol an interesting prototype for MRI-based PCa screening. It may also prove valuable as a follow-up tool in patients who cannot tolerate prolonged positioning in the MR scanner.

In Vivo Characterization

One of the primary goals of an imaging biomarker is to inform clinical decisions. In cancer, pathological grading is central to predicting tumor behavior. Due to the relatively high prevalence of clinically indolent tumors, distinguishing aggressive high grade tumors from lower grade lesions is particularly important for the appropriate management of PCa, as patients with lower grade disease may benefit from active surveillance rather than curative treatment.[52] Thus tools that can reliably distinguish low grade from high grade PCa are needed. RSI is well suited for evaluating tumor histopathology based on the fact that: cellularity maps can highlight intracellular water, reflecting tissue cellularity (Fig. 2) and the RSI CI signal should increase with increasing nuclear volume fraction (Fig. 4B). Both of these tissue characteristics play a role in histopathological grading.

In a retrospective analysis of 36 tumors from 28 patients,[39] Liss et al demonstrated that the RSI CI in aggressive PCa (primary Gleason score of ≥ 4) was statistically different from lower grade lesions (primary Gleason 3 or less), while ADC values trended toward, but did not achieve, statistical significance in this sample. This later result is likely attributable to the small number of patients in the study, as several prior studies have demonstrated a statistically significant correlation between primary Gleason grade and ADC value.[53,54] For example, in a study of 131 men who underwent 1.5T MRI with an endorectal coil before prostatectomy, Donati et al[53] demonstrated a Spearman coefficient of -0.36 when ADC value (b = 0,1000) was compared with Gleason grade. They also showed that 10th percentile ADC value can distinguish Gleason 6 from Gleason 7 lesions with and AUC of 0.76.[53]

Building upon the results of Liss et al,[39] McCammack et al[40] (described above) compared Gleason grade from 33 tumors as determined on whole-mount section to RSI cellularity, ADC, and K^{trans} map values derived from preoperative MRIs. Gleason grade was also compared with preoperative PSA levels. RSI CI had the closest correlation to Gleason grade (Spearman rank-order correlation coefficient (ρ) = 0.53), outperforming ADC maps (ρ = -0.42, negative value due to inverse relationship) and PSA levels (ρ = 0.36). An example case in which ADC was relatively equivocal while RSI was positive can be seen in Figure 7A. K^{trans} values did not significantly correlate with Gleason grade.[40] Further analysis of these data demonstrated a strong association between the upper quartile of the RSI CI for each ROI and primary Gleason grade (Fig. 8A). Thus RSI

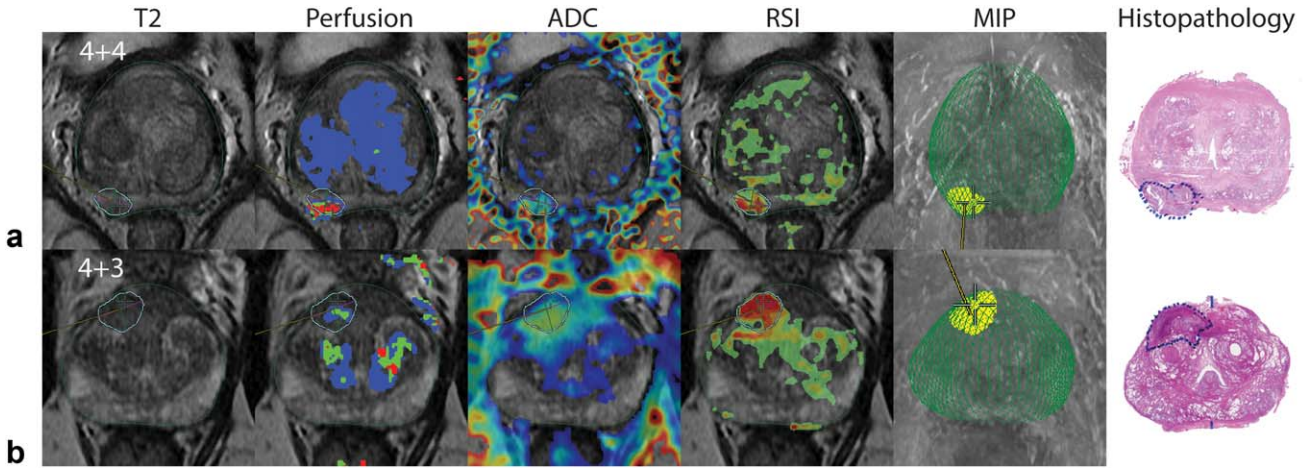

FIGURE 7: A: RSI guided biopsy where ADC is equivocal, but RSI clearly identifies the lesion. B: RSI guided biopsy finds high grade disease after repeated negative systematic biopsies. Modified with permission from McCammack et al. *PCAN* 2016.[40]

CI reliably and predictably correlates with underlying histopathology (Fig. 8B–D) (unpublished data).

Yamin et al further validated these findings at the voxel level. Regions of tumor were identified by a uropathologist on thin whole-mount sections from 10 patients with PCa with presurgical MR imaging. The sections were stained, scanned at high resolution (75 μm/pixel), and then divided into voxel size tiles. Each tile was graded on the Gleason scale and then compared with the RSI CI from preoperative MRI. In total 2795 individual tiles were reviewed and analyzed. On a voxel-by-voxel basis, RSI CI was significantly different among benign (mean RSI cellularity index = 0.16), low grade (mean score = 1.15) and high grade disease (mean score = 1.52) with increasing cellularity index correlating to increasing Gleason grade. Thus RSI CI correlates with Gleason grade at the voxel level, reflecting variation within individual tumors.[55]

Localization and Targeting

Once cancer has been detected by screening PSA or imaging, it must be confirmed by biopsy. Ultrasound-guided biopsy with a minimum of 10–12 cores systematically sampled from various regions of the prostate using a standard template remains the gold standard for PCa diagnosis.[52] However, the diagnostic yield of random systematic prostate biopsy remains limited, and variations between biopsy Gleason sum and surgery Gleason sum are relatively common. For example, in one study of 1113 men with prostate cancer diagnosed with systematic biopsy, 27% of cases were upgraded and 11% downgraded based on the radical prostatectomy specimen.[56]

Promising results have demonstrated that targeted biopsy using MRI, fused to ultrasound or using direct MRI guidance, may improve the detection of clinically significant disease while decreasing the diagnosis of clinically indolent disease.[57–59] One challenge with this approach is that targeted biopsies alone may miss clinically significant lesions found using current systematic biopsy methods.[58,59] This is thought to relate to imperfections in the diagnostic accuracy of current mpMRI protocols, both in distinguishing PCa from normal tissue and in identifying areas of high grade disease within the tumor. Areas of clinically relevant disease missed on imaging would naturally not be targeted for biopsy, while these sites may be found by chance using the systematic biopsy approach. In the prior sections "Cancer detection" and "In vivo characterization," we outlined data demonstrating the superior detection accuracy of RSI over current mpMRI, and showed that RSI CI strongly correlates

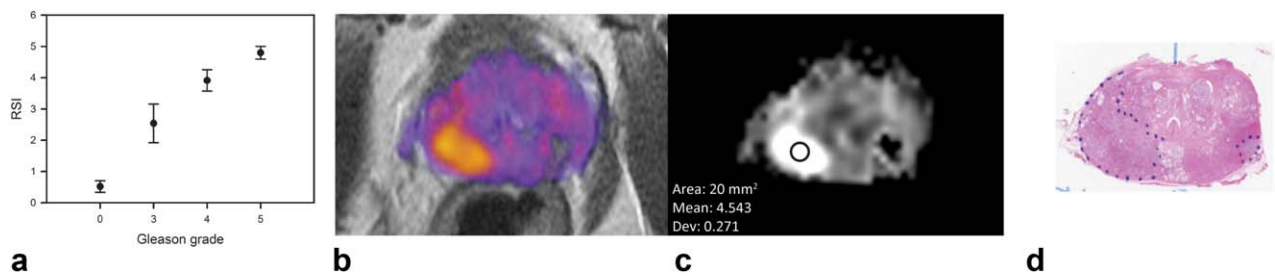

FIGURE 8: A: Correlation between primary Gleason score and RSI cellularity index, using the same data presented in McCammack et al. *PCAN*, 2016,[40] reanalyzed to show the top quartile for each ROI. Benign, 0–1.5; Primary 3, 1.5–3; Primary 4, 3–4.5; Primary 5, > 4.5. B: RSI cellularity map in color. C: RSI cellularity map in gray-scale, showing the RSI cellularity index for the indicated ROI. D: corresponding whole-mount histopathology slide with the tumor outline in blue.

with Gleason grade. This combination of assets suggests that areas of high-grade disease can be identified and directly targeted under RSI guidance, potentially increasing sampling yield and diagnostic accuracy while reducing the need for repeat procedures.

Distortion correction techniques also carry implications for targeted biopsies. Rakow-Penner et al developed distortion maps derived from direct comparison of pre- and postdistortion corrected images from preoperative MRIs of 27 PCa patients. Their findings demonstrate that uncorrected diffusion weighted images can have spatial registration errors of up to 13 mm (SD 3.1)[32] or up to one third of the prostate gland itself. Misregistration on that scale could have significant deleterious effects on targeted biopsy, as well as staging and treatment planning. Correction for spatial distortion opens the door to image-guided targeting of small volume lesions suspected to be high-grade disease. This would overcome one of the major limitations of systematic biopsy, which can miss smaller lesions.[60,61]

A previously published example demonstrates the power of this approach, with RSI guided-biopsy revealing Gleason 4 + 3 disease in a patient who had three previous negative systematic biopsies (Fig. 7B).[40] While systematic biopsy currently remains the gold standard for diagnosis in patients undergoing initial prostate biopsy, RSI can serve a role in identification of biopsy targets, particularly in patients who have undergone at least one prior negative prostate biopsy.[62]

Interpretation of Prostate MRI with RSI: Clinical Practice

The studies presented above demonstrate that the addition of RSI (mpMRI+RSI) provides superior diagnostic accuracy in both computer-based and clinical radiologist-based detection of prostate cancer as compared to current standard-of-care multiparametric MRI. Given these findings, we now incorporate the RSI sequence into all prostate MRIs at our institution, with the fused axial T2 + RSI cellularity maps forming the foundation for RSI interpretation (Fig. 5B). In practice, the same principle outlined for interpretation of ADC in the PIRADS version 2 (v2) guidelines are applied to the RSI cellularity map (RSI-CM). Information from the ADC map and RSI-CM are interpreted in conjunction for initial scoring of peripheral zone lesions; in keeping with PIRADS v2 principles (Fig. 9A). Conversely, transitional zone lesions are primarily scored using findings from T2w images with RSI-CM used in conjunction with ADC maps to further characterize T2w grade 3 lesions; also in line with PIRADS v2 guidelines (Fig. 9B). Moreover, the data outlined above also underscore that the RSI CI, derived from the RSI cellularity maps, strongly correlates with histopathological Gleason grade down to the voxel level. In light of these results we sometimes include a predicted Gleason score on MRI reports based on the RSI CI (Fig. 9C), as guided by data in Figure 8A. The reported RSI CI is determined by drawing an ROI that incorporates approximately half of the suspicious lesion, with care taken to avoid lesion margins. The RSI CI is tabulated from the top quartile cut-off within the ROI.

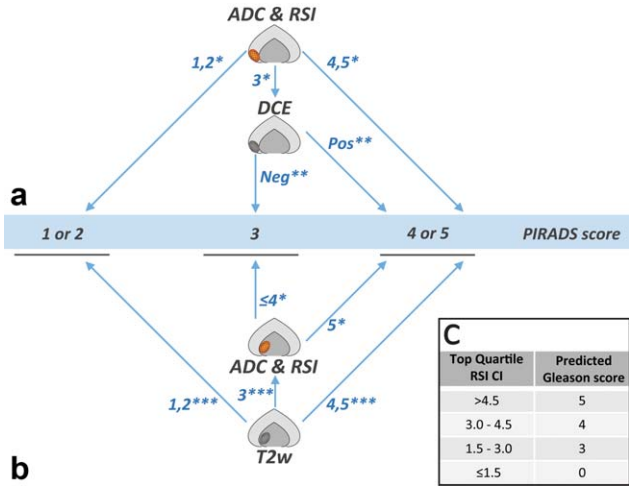

FIGURE 9: Proposed follow-up guidelines based on PIRADSv2 incorporating RSI-MRI. A: Peripheral zone. B: Transitional zone. C: Predicted Gleason score based on RSI Cellularity index (CI). *using PIRADSv2 guidelines for conventional DWI; **using PIRADSv2 guidelines for dynamic contrast enhancement; ***using PIRADSv2 guidelines for T2-weighted images

Future Applications

As discussed above, there is great interest in developing robust, cost-effective, prostate cancer screening tools. The work by McCammack et al[41](see Cancer Detection section) demonstrated that an abbreviated protocol combining RSI and T2w images alone is as sensitive in detecting prostate cancer as mpMRI. This protocol can be acquired in less than 10 min on a GE Signa HDx 3T scanner, with the potential for even faster times on more modern systems. One of the major critiques of using MRI as a screening tool is the cost. As a significant portion of the cost of MRI is attributable to the length of acquisitions, shorter protocols could lead to a decrease in the cost of an MRI. Moreover, limiting the number of sequences should increase the speed of interpretation, which may provide an additional source of cost savings. Future efforts will be needed to determine if this abbreviated RSI + T2w protocol can offer an alternative to current screening methods.

An added benefit of using MRI for screening is that images can subsequently be used for targeted biopsy. The above-described distortion correction techniques combined with improved diagnostic performance over conventional MRI tools suggest that RSI is well suited for image-guided biopsy and targeted therapy. Thus, fast acquisition RSI-based screening studies could subsequently be used for biopsy guidance with increased diagnostic yield and assist in

treatment plan development at no additional cost. Direct comparison of RSI-guided biopsy against current standard-of-care systematic biopsy will be needed.

Future studies should be aimed at vetting the association between Gleason grade and RSI CI. With further refinement there may be instances where imaging-based evaluation of tumors will obviate the need for biopsy altogether leading to additional cost savings while avoiding the small, but not inconsequential, risk of complications following biopsy.

DWI evaluation of prostatic lesions is sometimes complicated by hemorrhage and inflammation post biopsy.[29] However, as discussed previously, RSI is specific for areas of high cellularity (Figs. 3 and 5B) and should be less susceptible to the effects of extracellular edema or blood products. This concept was validated in a small study of patients with CNS neoplasms, wherein RSI was superior to DTI in delineating normal white matter tracts in the setting of peritumoral FLAIR hyperintensity,[48] demonstrating the ability of RSI to identify meaningful pathology despite regional inflammation. Early clinical experience suggests a similar trend in prostate cancer patients (unpublished data).

The principles that make diffusion-based techniques attractive in prostate cancer are readily applied to other neoplasms. DWI is now included in routine MR protocols for oncologic imaging at institutions around the world,[63,64] with a strong correlation to tissue cellularity[65] and prognosis[36] in many abdominal and pelvic malignancies in addition to PCa. Despite these results, ADC values remain difficult to apply in the clinical setting for reasons outlined above, namely overlapping reference ranges and variable reproducibility. RSI is currently being evaluated in several abdominal and pelvic cancers where ADC maps have demonstrated clinical utility: in cervical cancer to evaluate for parametrial invasion,[66] in rectal cancer to evaluate for extension through the mesorectal fascia,[67] and in several tumor types for identifying pathological lymph nodes.[68] RSI also has a potential role in evaluating suspicious renal lesions. Oncocytomas in particular, present an important diagnostic dilemma as these lesions can appear indistinguishable from renal cell carcinoma on CT[69] and anatomic MR[70] sequences, yet are benign lesions that generally do not require surgery.[71] Other areas of active research include early posttreatment assessment and whole body MRI.

Limitations

Like all diffusion-based techniques, RSI suffers from low resolution and in most settings will be best used as an adjunct to high spatial resolution sequences. Additionally, some normal structures such as the spleen and spinal cord show inherently high signal on RSI cellularity maps (Fig. 10). Thus, RSI will be best applied as part of a multiparametric / multimodal imaging protocol.

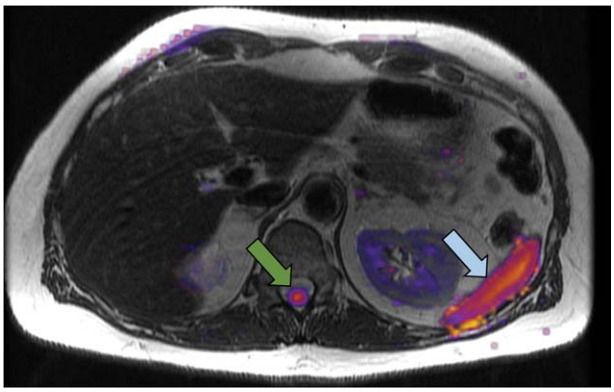

FIGURE 10: Limitations of RSI: normal structures with high signal on the RSI cellularity map include the spinal cord (green arrow) and the spleen (blue arrow).

The application of RSI to PCa has been designed to highlight the highly restricted isotropic water found in epithelial cells. The findings that RSI CI correlates with Gleason grade match segmentation studies wherein increasing epithelial cell number correlated positively with increasing Gleason grade.[72] However, other pathological changes such as decreased stromal tissue and decreased luminal space have also been shown to correlate with increasing Gleason grade,[72] highlighting the complex nature of the architectural changes that occur during neoplastic dedifferentiation. Thus, another limitation of RSI is that it may fail to identify some of the histopathologic features that characterize increasing Gleason grade.

While the strength of RSI comes from being able to isolate specific water fractions (e.g., intracellular water), other diffusion-based techniques may prove more powerful for certain pathological settings not focused on identifying highly cellular tissues. For example, conventional DWI proves to be better than RSI at identifying edema in patients with CNS malignancy.[45] Future studies will be needed to clarify the pathological questions best suited to each unique diffusion-based technique.

ADC values are technique and machine dependent.[36,37] This limits if not precludes the development of generalizable parameters and reference ranges, a critical step in the development of an effective imaging biomarker.[34] While partially addressed by the normalization steps used in calculating RSI cellularity maps, RSI techniques will need to be standardized to avoid the technique variability that has constrained comparison of ADC maps across sites.

Image distortion is a critical issue in the translation of imaging findings to clinically actionable information. Differences on the scale of a millimeter can result in changes in treatment plans. Thus the vetting and continued refinement of distortion correction tools will be vital to the implementation of RSI in guiding patient care.

Focused efforts should initially be aimed at those tumors where compelling data exists from the ADC literature, as some cancer patients may not benefit from RSI or other advanced diffusion-based techniques. For example,

evaluation of pulmonary nodules with DWI have had mixed results. One study demonstrated no difference in ADC values between 18 malignant pulmonary nodules and 10 benign nodules,[73] and a meta-analysis by Li et al raised questions about the clinical utility of DWI in evaluating pulmonary nodules.[74] While usage of DWI contrast ratios between the lesion in question and an internal control (for example, the spinal cord)[73,75] may help resolve some of these issues, it is important to keep in mind that no single tool will be adequate for all oncologic imaging.

In conclusion, diffusion-weighted imaging has proven utility in PCa. Results to date suggest that RSI can build upon the success of conventional DWI while addressing several known limitations. RSI isolates signal from isotropic restricted volumes of water to highlight regions of cellularity with high conspicuity making it a powerful tool in PCa detection and localization. An abbreviated protocol combining RSI and an anatomic T2-weighted image may offer a viable option for imaging-based PCa screening, using a decision tree developed on current PIRADSv2 recommendations. RSI CI strongly correlates with Gleason grade making imaging-based in vivo characterization a reality, while robust distortion correction techniques allow RSI data to be clinically applied in the setting of cancer staging, image-guided targeted biopsy or therapy. With the advent of RSI, combined with the continued development of other imaging techniques, new standards in the early detection of malignancy and improved therapeutic guidance are on the horizon.

Acknowledgments

Contract grant sponsor: Department of Defense (DoD); contract grant number: W81XWH-13-1-0391; Contract grant sponsor: the American Cancer Society; contract grant number: 70-002; Contract grant sponsor: UCSD Clinician Scientist Program; contract grant number: 5T32EB005970-07; Contract grant sponsor: NINDS P30 core grant; contract grant number: NS047101; Contract grant sponsor: General Electric, Investigator Initiated Research Award; contract grant number: BOK92325

This study was funded by a Department of Defense (DoD) grant, Prostate Cancer Research Program, the American Cancer Society Institutional Research Grant, UCSD Clinician Scientist Program, UCSD School of Medicine Microscopy Core, and NINDS P30 core grant, and a General Electric, Investigator Initiated Research Award.

References

1. American Cancer Society. Cancer facts and figures. Atlanta, GA: American Cancer Society; 2016.
2. SEER Stat Fact Sheet. Surveillance, epidemiology, and end results program. Bethesda, MD: National Cancer Institute.
3. Ueno Y, Tamada T, Bist V, et al. Multiparametric magnetic resonance imaging: Current role in prostate cancer management. Int J Urol 2016;23:550–557.
4. Oppenheimer DC, Weinberg EP, Hollenberg GM, Meyers SP. Multiparametric magnetic resonance imaging of recurrent prostate cancer. J Clin Imaging Sci 2016;6:18.
5. Felker ER, Margolis DJ, Nassiri N, Marks LS. Prostate cancer risk stratification with magnetic resonance imaging. Urol Oncol 2016;34:311–319.
6. Park JJ, Kim CK, Park SY, Park BK, Lee HM, Cho SW. Prostate cancer: role of pretreatment multiparametric 3-T MRI in predicting biochemical recurrence after radical prostatectomy. AJR Am J Roentgenol 2014;202:W459–W465.
7. Futterer JJ, Briganti A, De Visschere P, et al. Can clinically significant prostate cancer be detected with multiparametric magnetic resonance imaging?. A systematic review of the literature. Eur Urol 2015;68:1045–1053.
8. Hegde JV, Mulkern RV, Panych LP, et al. Multiparametric MRI of prostate cancer: an update on state-of-the-art techniques and their performance in detecting and localizing prostate cancer. J Magn Reson Imaging 2013;37:1035–1054.
9. Isebaert S, Van den Bergh L, Haustermans K, et al. Multiparametric MRI for prostate cancer localization in correlation to whole-mount histopathology. J Magn Reson Imaging 2013;37:1392–1401.
10. Kitajima K, Kaji Y, Fukabori Y, Yoshida K, Suganuma N, Sugimura K. Prostate cancer detection with 3 T MRI: comparison of diffusion-weighted imaging and dynamic contrast-enhanced MRI in combination with T2-weighted imaging. J Magn Reson Imaging 2010;31:625–631.
11. Lim HK, Kim JK, Kim KA, Cho KS. Prostate cancer: apparent diffusion coefficient map with T2-weighted images for detection--a multireader study. Radiology 2009;250:145–151.
12. Haider MA, van der Kwast TH, Tanguay J, et al. Combined T2-weighted and diffusion-weighted MRI for localization of prostate cancer. AJR Am J Roentgenol 2007;189:323–328.
13. Donati OF, Jung SI, Vargas HA, et al. Multiparametric prostate MR imaging with T2-weighted, diffusion-weighted, and dynamic contrast-enhanced sequences: are all pulse sequences necessary to detect locally recurrent prostate cancer after radiation therapy? Radiology 2013;268:440–450.
14. Turkbey B, Pinto PA, Mani H, et al. Prostate cancer: value of multiparametric MR imaging at 3 T for detection--histopathologic correlation. Radiology 2010;255:89–99.
15. Giannarini G, Nguyen DP, Thalmann GN, Thoeny HC. Diffusion-weighted magnetic resonance imaging detects local recurrence after radical prostatectomy: initial experience. Eur Urol 2012;61:616–620.
16. Miao H, Fukatsu H, Ishigaki T. Prostate cancer detection with 3-T MRI: comparison of diffusion-weighted and T2-weighted imaging. Eur J Radiol 2007;61:297–302.
17. Tan CH, Wei W, Johnson V, Kundra V. Diffusion-weighted MRI in the detection of prostate cancer: meta-analysis. AJR Am J Roentgenol 2012;199:822–829.
18. Langer DL, van der Kwast TH, Evans AJ, Trachtenberg J, Wilson BC, Haider MA. Prostate cancer detection with multi-parametric MRI: logistic regression analysis of quantitative T2, diffusion-weighted imaging, and dynamic contrast-enhanced MRI. J Magn Reson Imaging 2009;30:327–334.
19. Peng Y, Jiang Y, Yang C, et al. Quantitative analysis of multiparametric prostate MR images: differentiation between prostate cancer and normal tissue and correlation with Gleason score--a computer-aided diagnosis development study. Radiology 2013;267:787–796.
20. Peng Y, Jiang Y, Antic T, Giger ML, Eggener SE, Oto A. Validation of quantitative analysis of multiparametric prostate MR images for

prostate cancer detection and aggressiveness assessment: a cross-imager study. Radiology 2014;271:461–471.

21. Kozlowski P, Chang SD, Jones EC, Berean KW, Chen H, Goldenberg SL. Combined diffusion-weighted and dynamic contrast-enhanced MRI for prostate cancer diagnosis--correlation with biopsy and histopathology. J Magn Reson Imaging 2006;24:108–113.
22. Vargas HA, Hotker AM, Goldman DA, et al. Updated prostate imaging reporting and data system (PIRADS v2) recommendations for the detection of clinically significant prostate cancer using multiparametric MRI: critical evaluation using whole-mount pathology as standard of reference. Eur Radiol 2016;26:1606–1612.
23. Turkbey B, Choyke PL. PIRADS 2.0: what is new? Diagn Interv Radiol 2015;21:382–384.
24. White NS, Leergaard TB, D'Arceuil H, Bjaalie JG, Dale AM. Probing tissue microstructure with restriction spectrum imaging: Histological and theoretical validation. Hum Brain Mapp 2013;34:327–346.
25. Le Bihan D. Molecular diffusion, tissue microdynamics and microstructure. NMR Biomed 1995;8:375–386.
26. Le Bihan D, Mangin J-F, Poupon C, et al. Diffusion tensor imaging: Concepts and applications. J Magn Reson Imaging 2001;13:534–546.
27. Yamada K, Sakai K, Akazawa K, Yuen S, Nishimura T. MR tractography: a review of its clinical applications. Magn Reson Med Sci 2009;8: 165–174.
28. Stejskal EO, Tanner JE. Spin diffusion measurement: spin echoes in the presence of a time dependent field gradient. J Chem Phys 1965; 42:288–292.
29. Tamada T, Sone T, Jo Y, et al. Prostate cancer: relationships between postbiopsy hemorrhage and tumor detectability at MR diagnosis. Radiology 2008;248:531–539.
30. Donato F Jr, Costa DN, Yuan Q, Rofsky NM, Lenkinski RE, Pedrosa I. Geometric distortion in diffusion-weighted MR imaging of the prostate-contributing factors and strategies for improvement. Acad Radiol 2014;21:817–823.
31. White NS, Dale AM. Distinct effects of nuclear volume fraction and cell diameter on high b-value diffusion MRI contrast in tumors. Magn Reson Med 2014;72:1435–1443.
32. Rakow-Penner RA, White NS, Margolis DJ, et al. Prostate diffusion imaging with distortion correction. Magn Reson Imaging 2015;33: 1178–1181.
33. White NS, McDonald C, Farid N, et al. Diffusion-weighted imaging in cancer: physical foundations and applications of restriction spectrum imaging. Cancer Res 2014;74:4638–4652.
34. Prescott JW. Quantitative imaging biomarkers: the application of advanced image processing and analysis to clinical and preclinical decision making. J Digit Imaging 2013;26:97–108.
35. Jung KH, Lee KH. Molecular imaging in the era of personalized medicine. J Pathol Transl Med 2015;49:5–12.
36. Heijmen L, Verstappen MC, Ter Voert EE, et al. Tumour response prediction by diffusion-weighted MR imaging: ready for clinical use? Crit Rev Oncol Hematol 2012;83:194–207.
37. Jie C, Rongbo L, Ping T. The value of diffusion-weighted imaging in the detection of prostate cancer: a meta-analysis. Eur Radiol 2014;24: 1929–1941.
38. Schreuder SM, Lensing R, Stoker J, Bipat S. Monitoring treatment response in patients undergoing chemoradiotherapy for locally advanced uterine cervical cancer by additional diffusion-weighted imaging: A systematic review. J Magn Reson Imaging 2014;42:572–594.
39. Liss MA, White NS, Parsons JK, et al. MRI-derived restriction spectrum imaging cellularity index is associated with high grade prostate cancer on radical prostatectomy specimens. Front Oncol 2015;5:30.
40. McCammack KC, Kane CJ, Parsons JK, et al. In vivo prostate cancer detection and grading using restriction spectrum imaging-MRI. Prostate Cancer Prostatic Dis 2016;19:168–173.
41. McCammack KC, Schenker-Ahmed NM, White NS, et al. Restriction spectrum imaging improves MRI-based prostate cancer detection. Abdom Radiol (NY) 2016;41:946–953.
42. de Rooij M, Hamoen EH, Witjes JA, Barentsz JO, Rovers MM. Accuracy of magnetic resonance imaging for local staging of prostate cancer: a diagnostic meta-analysis. Eur Urol 2016;70:233–245.
43. Holland D, Kuperman JM, Dale AM. Efficient correction of inhomogeneous static magnetic field-induced distortion in Echo Planar Imaging. Neuroimage 2010;50:175–183.
44. Rakow-Penner RA, White NS, Parsons JK, et al. Novel technique for characterizing prostate cancer utilizing MRI restriction spectrum imaging: proof of principle and initial clinical experience with extraprostatic extension. Prostate Cancer Prostatic Dis 2015;18:81–85.
45. Farid N, Almeida-Freitas DB, White NS, et al. Combining diffusion and perfusion differentiates tumor from bevacizumab-related imaging abnormality (bria). J Neurooncol 2014;120:539–546.
46. Farid N, Almeida-Freitas DB, White NS, et al. Restriction-spectrum imaging of bevacizumab-related necrosis in a patient with GBM. Front Oncol 2013;3:258.
47. McDonald CR, Delfanti RL, Krishnan AP, et al. Restriction spectrum imaging predicts response to bevacizumab in patients with high-grade glioma. Neuro Oncol 2016 [Epub ahead of print].
48. McDonald CR, White NS, Farid N, et al. Recovery of white matter tracts in regions of peritumoral FLAIR hyperintensity with use of restriction spectrum imaging. AJNR Am J Neuroradiol 2013;34:1157–1163.
49. White NS, McDonald CR, Farid N, Kuperman JM, Kesari S, Dale AM. Improved conspicuity and delineation of high-grade primary and metastatic brain tumors using "restriction spectrum imaging": quantitative comparison with high B-value DWI and ADC. AJNR Am J Neuroradiol 2013;34:958–964, S1.
50. Hygino da Cruz LC Jr, Rodriguez I, Domingues RC, Gasparetto EL, Sorensen AG. Pseudoprogression and pseudoresponse: imaging challenges in the assessment of posttreatment glioma. AJNR Am J Neuroradiol 2011;32:1978–1985.
51. Mong S, Ellingson BM, Nghiemphu PL, et al. Persistent diffusion-restricted lesions in bevacizumab-treated malignant gliomas are associated with improved survival compared with matched controls. AJNR Am J Neuroradiol 2012;33:1763–1770.
52. McDonald ML, Parsons JK. The case for tailored prostate cancer screening: an NCCN perspective. J Natl Compr Canc Netw 2015;13: 1576–1583.
53. Donati OF, Mazaheri Y, Afaq A, et al. Prostate cancer aggressiveness: assessment with whole-lesion histogram analysis of the apparent diffusion coefficient. Radiology 2014;271:143–152.
54. Vargas HA, Akin O, Franiel T, et al. Diffusion-weighted endorectal MR imaging at 3 T for prostate cancer: tumor detection and assessment of aggressiveness. Radiology 2011;259:775–784.
55. Yamin G, Schenker-Ahmed NM, Shabaik A, et al. Voxel level radiologic-pathologic validation of Restriction Spectrum Imaging cellularity index with Gleason grade in Prostate Cancer. Clin Cancer Res 2016;22:2668–2674.
56. Freedland SJ, Kane CJ, Amling CL, et al. Upgrading and downgrading of prostate needle biopsy specimens: risk factors and clinical implications. Urology 2007;69:495–499.
57. Murphy G, Haider M, Ghai S, Sreeharsha B. The expanding role of MRI in prostate cancer. AJR Am J Roentgenol 2013;201:1229–1238.
58. Siddiqui MM, Rais-Bahrami S, Turkbey B, et al. Comparison of MR/ultrasound fusion-guided biopsy with ultrasound-guided biopsy for the diagnosis of prostate cancer. JAMA 2015;313:390–397.
59. Siddiqui MM, Rais-Bahrami S, Truong H, et al. Magnetic resonance imaging/ultrasound-fusion biopsy significantly upgrades prostate cancer versus systematic 12-core transrectal ultrasound biopsy. Eur Urol 2013;64:713–719.
60. Vourganti S, Rastinehad A, Yerram NK, et al. Multiparametric magnetic resonance imaging and ultrasound fusion biopsy detect prostate

cancer in patients with prior negative transrectal ultrasound biopsies. J Urol 2012;188:2152–2157.

61. Sonn GA, Chang E, Natarajan S, et al. Value of targeted prostate biopsy using magnetic resonance-ultrasound fusion in men with prior negative biopsy and elevated prostate-specific antigen. Eur Urol 2014;65:809–815.
62. Carroll PR, Parsons JK, Andriole G, et al. NCCN Guidelines insights: prostate cancer early detection, version 2.2016. J Natl Compr Canc Netw 2016;14:509–519.
63. Koh DM, Lee JM, Bittencourt LK, Blackledge M, Collins DJ. Body diffusion-weighted MR imaging in oncology: imaging at 3T. Magn Reson Imaging Clin N Am 2016;24:31–44.
64. Jafar MM, Parsai A, Miquel ME. Diffusion-weighted magnetic resonance imaging in cancer: Reported apparent diffusion coefficients, in-vitro and in-vivo reproducibility. World J Radiol 2016;8:21–49.
65. Chen L, Liu M, Bao J, et al. The correlation between apparent diffusion coefficient and tumor cellularity in patients: a meta-analysis. PLoS One 2013;8:e79008.
66. Dhanda S, Thakur M, Kerkar R, Jagmohan P. Diffusion-weighted imaging of gynecologic tumors: diagnostic pearls and potential pitfalls. Radiographics 2014;34:1393–1416.
67. Burdan F, Sudol-Szopinska I, Staroslawska E, et al. Magnetic resonance imaging and endorectal ultrasound for diagnosis of rectal lesions. Eur J Med Res 2015;20:4.
68. Bonekamp S, Corona-Villalobos CP, Kamel IR. Oncologic applications of diffusion-weighted MRI in the body. J Magn Reson Imaging 2012;35:257–279.
69. Choudhary S, Rajesh A, Mayer NJ, Mulcahy KA, Haroon A. Renal oncocytoma: CT features cannot reliably distinguish oncocytoma from other renal neoplasms. Clin Radiol 2009;64:517–522.
70. Rosenkrantz AB, Hindman N, Fitzgerald EF, Niver BE, Melamed J, Babb JS. MRI features of renal oncocytoma and chromophobe renal cell carcinoma. AJR Am J Roentgenol 2010;195:W421–W427.
71. Ng KL, Rajandram R, Morais C, et al. Differentiation of oncocytoma from chromophobe renal cell carcinoma (RCC): can novel molecular biomarkers help solve an old problem? J Clin Pathol 2014;67:97–104.
72. Chatterjee A, Watson G, Myint E, Sved P, McEntee M, Bourne R. Changes in epithelium, stroma, and lumen space correlate more strongly with Gleason pattern and are stronger predictors of prostate ADC changes than cellularity metrics. Radiology 2015;277:751–762.
73. Uto T, Takehara Y, Nakamura Y, et al. Higher sensitivity and specificity for diffusion-weighted imaging of malignant lung lesions without apparent diffusion coefficient quantification. Radiology 2009;252:247–254.
74. Li B, Li Q, Chen C, Guan Y, Liu S. A systematic review and meta-analysis of the accuracy of diffusion-weighted MRI in the detection of malignant pulmonary nodules and masses. Acad Radiol 2014;21:21–29.
75. Nomori H, Cong Y, Sugimura H, Kato Y. Comparing diffusion-weighted imaging and positron emission tomography for pulmonary nodules measuring from 1 to 3 cm in size. Surg Today 2015;45:1535–1541.